ELSEVIER

Journal of Nuclear Materials 277 (2000) 159–168

journal of nuclear materials

www.elsevier.nl/locate/jnucmat

Ion beam-induced amorphisation of freudenbergite

Katherine L. Smith[a,*], Mark G. Blackford[a], Gregory R. Lumpkin[a], Nestor J. Zaluzec[b]

[a] *Materials Division, Australian Nuclear Science and Technology Organisation, P.M.B. 1, Menai NSW 2234, Australia*
[b] *Materials Science Division, Argonne National Laboratory, 9700 South Cass Ave., Argonne Il, USA*

Received 29 March 1999; accepted 2 August 1999

Abstract

Using the HVEM-tandem facility at Argonne National Laboratory, the critical dose of 1.5 MeV Kr^+ ions for amorphisation of freudenbergite (D_c (freudenbergite)) at room temperature was found to be $1.6 \pm 0.3 \times 10^{18}$ ions m^{-2}. D_c (freudenbergite) is lower than D_c (zirconolite) and D_c (perovskite) (3.5–5.5 and 3.9–9.2×10^{18} ion m^{-2}, respectively). Freudenbergite can occur in Synroc-C, a titanate wasteform designed for immobilising high level radioactive waste (HLW). In Synroc-C, zirconolite and perovskite will contain the majority of the actinides in HLW. Freudenbergite will contain less than 0.2 wt% actinides but will experience displacement damage due to the alpha decay of actinides in surrounding phases. In agreement with the experimental findings of previous authors, our calculations show that in Synroc-C, freudenbergite will remain crystalline after zirconolite and perovskite have become amorphous. Neither of the two current parameters (structural freedom, f or susceptibility to amorphisation, S) for estimating the relative radiation resistance of different phases is capable of predicting the relative radiation resistance of freudenbergite, zirconolite and perovskite. The low D_c of freudenbergite may result from Na^+ ions having significantly lower E_d values compared to the other elements in freudenbergite, zirconolite and perovskite, in the electric fields induced by heavy ion irradiation of TEM specimens. If this hypothesis is true, it challenges the assumption that heavy ion irradiation can be used to compare the relative radiation resistance of different phases and will have serious implications for the predictive parameters of radiation resistance.

PACS: 61.80.-x; 61.80.Jh; 61.72.Ff; 81.05.Je

1. Introduction

Synroc is a polyphase titanate ceramic designed for the immobilisation of high level radioactive waste (HLW) [1]. In standard Synroc-C, ionic fission products are held in solid solution in zirconolite ($CaZrTi_2O_7$, [2]), perovskite ($CaTiO_3$, [3]) and hollandite ((Ba_x, Cs_y)[$(Al,Ti^{3+})_{2x+y}(Ti^{4+}_{8-2x-y})$]$_8O_{16}$), with the actinides partitioning into zirconolite and perovskite. Sodium is not a fission product but is often present in HLW for three reasons: NaOH is added to neutralise waste after re-processing, and $NaNO_3$ and Na_2CO_3 are added during reprocessing for redox control and to refurbish organic solvents damaged by irradiation, respectively. More than ~1.5 wt% of Na in standard Synroc-C ceramics can result in: (i) the formation of water-soluble Na-rich intergranular films [4], (ii) additional phases [4–6] which can result in reduced durability [5–7] and (iii) the formation of loparite (sodium and rare-earth-element bearing perovskite) which also increases the fractionation of actinides into perovskite [8], the least durable of the major Synroc phases.

Freudenbergite ($Na_2(Al, Fe, Ti)_2Ti_6O_{16}$, [9,10]) occurs in Synrocs containing $\leqslant 1.2$ wt% Na_2O [8]. Its leach rate is >0.01 g/m^2/day in deionised water at 90°C [11], which is comparable to the leach rate of perovskite containing Na and rare earth elements (REEs) [12]. In

* Corresponding author. Tel.: +61-2 9717 3505; fax: +61-2 9543 7179.
E-mail address: kls@ansto.gov.au (K.L. Smith).

0022-3115/00/$ - see front matter
PII: S0022-3115(99)00210-X

Synroc-C, freudenbergite will contain less than 0.2 wt% actinides [8] and consequently it will not experience much self-induced alpha decay damage. However freudenbergite will experience ionisation and displacement damage due to the transit of α-particles and long-range β- and γ-rays and the incursion of α-recoil nuclei from neighbouring grains of zirconolite and perovskite.

Vance et al. [11] investigated freudenbergite's resistance to ionising radiation by irradiating samples with 200 kV electrons using a transmission electron microscope (TEM). They found that freudenbergite remains crystalline even after receiving an electron dose an order of magnitude higher than that required to amorphise quartz. Previously Roberts et al. [13] showed that the cumulative ionisation damage experienced by Synroc-C 10^4–10^6 years after fabrication will be 10^{10} Gy and Pacuscci et al. [14] found that quartz became fully amorphous at 10^{12} Gy. Consequently, as Vance et al. [11] argued, freudenbergite is an acceptable component of Synroc-type ceramics, on the basis of its durability and resistance to ionising radiation.

In this study, freudenbergite's response to displacement damage is investigated by irradiation with 1.5 MeV Kr^+ ions. The critical dose for amorphisation, D_c, is established in situ by electron diffraction and compared to the critical amorphisation doses of zirconolite and perovskite. Finally, the theoretical parameters f and S for prediction of the relative resistance of different phases to radiation damage are calculated and discussed.

2. Experimental procedure

The material used in this study is the targeted end-member freudenbergite, $Na_2Al_2Ti_6O_{16}$, made by Vance et al. [11]. Using a scanning electron microscope fitted with an energy dispersive spectrometer, we found that the sample is predominantly freudenbergite ($Na_{1.91}Al_{1.88}Ti_{6.14}O_{16.06}$), with a minor amount of a second Al-rich (Na, Al, Ti)-oxide phase.

TEM specimens were prepared by crushing material under ethanol then passing holey carbon grids through the suspension and collecting fine particles on the carbon film. As freudenbergite is not the sole phase present in the fabricated material, the positions of freudenbergite grains on TEM grids were mapped on secondary electron images (SEIs) of the grids collected using a JEOL 2000 FX analytical TEM equipped with an ASID scanning attachment and a hybrid energy dispersive spectrometer [15]. To prevent any electron damage during the mapping and identification process, the electron flux was kept below 3×10^{23} e m^{-2} s^{-1} at all times to prevent ionisation damage [11].

In situ ion irradiation of the TEM specimens was performed using a 1.2 MeV modified Kratos/AEI EM7 electron microscope (operated at 300 kV) interfaced with an NEC ion accelerator in the HVEM-Tandem User Facility at Argonne National Laboratory. All irradiation experiments were conducted nominally at room temperature. In similar experiments we conducted at room temperature the monitored temperature of the grid did not rise above 50°C during irradiations. Grains selected for ion irradiation showed many maxima in their selected area electron diffraction (SAD) patterns. The monitored areas of these grains had thicknesses of ~1500 Å. The integrated electron flux experienced by TEM grids in this apparatus was always $\leqslant 1 \times 10^{18}$ e m^{-2} s^{-1} (i.e., the integrated electron flux was $\sim 10^8$ times lower that which caused damage in a previous study [11]). Specimens were irradiated with 1.5 MeV Kr^+ ions using the procedure described by Smith et al. [16]. For each monitored grain, the average of the dose at which all Bragg reflections had disappeared and the dose immediately prior to that dose was taken to be the critical dose for amorphisation, D_c.

3. Results

Ten freudenbergite grains were monitored. One of the monitored grains was found to be an outlier (i.e., it retained a degree of crystallinity after it had received much higher doses than that required to make amorphous other freudenbergite grains in the vicinity [16]). Smith et al. [16] suggested that the apparent radiation resistance of outliers is due to poor thermal connection between the individual grain and the holey carbon film. In agreement with common practice, we discarded the data from the outlier. From the remaining data, taking D_c to be the average of the dose at which all Bragg reflections had disappeared and the dose immediately prior to that dose, we calculate D_c (freudenbergite) to be $1.6 \pm 0.3 \times 10^{18}$ ions m^2. The quoted error in D_c values reflects the spread of experimental results.

4. Discussion

4.1. The relative radiation resistance of freudenbergite and the actinide-bearing phases in modified Synroc-C

As stated in the introduction, freudenbergite in modified Synroc-C contains less than 0.2 wt% actinides. Consequently most of the displacement damage in freudenbergite will result from the incursion of α-recoil nuclei and the transit of α-particles generated in adjacent actinide-bearing grains (zirconolite and perovskite).

The highest level of displacement damage in freudenbergite grains in modified Synroc-C will occur at the edges of the grains, for two reasons. Firstly, a narrow band at the periphery of freudenbergite grains will suffer displacement damage due to the incursion of α-recoil nuclei from neighbouring actinide-bearing grains. The

band will be narrow because the range of α-recoil nuclei in Synroc phases is only small (0.2 μm, [1]) in comparison to the size of freudenbergite grains (~0.5 μm). Secondly, the displacement damage due to α-particles will be distributed more or less uniformly throughout all the phases, because the grain size of Synroc-C fabricated under standard conditions (hot-pressing at 1250°C for 12 h at 21 MPa) is 0.2–1.0 μm, whereas the range of α-particles in Synroc is 10–20 μm [1].

If the thin, heavily damaged bands at the edges of freudenbergite grains were to become amorphous prior to adjacent actinide-bearing grains, they could act as diffusion pathways and adversely affect the durability of modified Synroc-C. Consequently, it is important to ascertain if the heavily damaged bands in freudenbergite will become amorphous before the actinide-bearing phases in Synroc-C.

In the following sections we do various calculations, with the final object of determining whether freudenbergite will retain its crystallinity for as long as the actinide-bearing phases in Synroc-C. In the first section we will estimate the amount of displacement damage caused by this incursion of α-recoil nuclei into the periphery of freudenbergite grains relative to that caused by α-recoil nuclei in the actinide-bearing phases. In the second section we will discuss and calculate the ratio of the amount of displacement damage caused by α-recoil nuclei and α-particles in Synroc phases. In the third section we will estimate the displacement damage in freudenbergite relative to that in zirconolite and perovskite.

4.1.1. Calculation of displacement damage in the periphery of freudenbergite grains caused by α-recoil nuclei from adjacent actinide-bearing phases

In order to estimate the amount of displacement damage in the periphery of freudenbergite grains in modified Synroc-C, caused by the incursion of α-recoil nuclei from neighbouring actinide-bearing, let us assume that the interface between freudenbergite grains and zirconolite or perovskite grains is flat (see Fig. 1(a)) and that recoil nuclei are uniformly distributed in angle. Then the recoil nuclei reaching point $P = (x_0, y_0, z_0)$ inside freudenbergite grains must have come from points in the adjacent zirconolite or perovskite grain with coordinates

$$x = l\sin\theta\cos\phi + x_0, \tag{1}$$

$$y = l\sin\theta\sin\phi + y_0, \tag{2}$$

$$z = l\cos\theta + z_0, \tag{3}$$

where l is the range of the average recoil nuclei, and θ and ϕ the angles as shown in Fig. 1. Therefore the total number of recoil nuclei (T) reaching P is

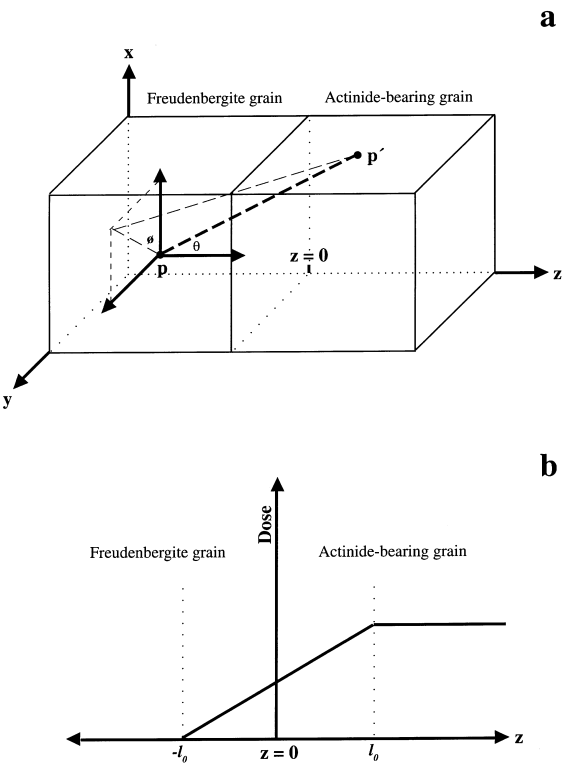

Fig. 1. (a) Simplified diagram of the interface between a freudenbergite grain and an actinide-bearing grain in Synroc-C. (b) Dose as a function of distance from the interface between a freudenbergite grain and an actinide-bearing grain in Synroc-C. See Section 4.1.2 for full explanation.

$$T = \int\int l^2\sin\theta\ \mathrm{d}\theta\ \mathrm{d}\phi \tag{4}$$

such that $z > 0$. That is

$$T = \int_0^{2\pi} \mathrm{d}\phi \int_0^{\arccos(-z_0/l)} l^2\sin\theta\ \mathrm{d}\theta \tag{5}$$

which has a linear solution:

$$T = 2\pi l^2[1 - (-z_0/l)] \tag{6}$$

from $z = l_0$ to $z = -l_0$.

This solution is diagrammatically represented in Fig. 1(b). From this figure, it can be seen that the average dose due to alpha recoils in the periphery of freudenbergite grains is one quarter of the dose in surrounding actinide-bearing grains, as calculated directly from the actinide content, assuming it is uniformly distributed throughout the grains. Note also that the average dose in the periphery of the actinide-bearing grains is three quarters of the dose in the interior of those grains.

4.1.2. Calculations of damage induced by recoil nuclei and alpha particles in Synroc phases

Reeve and Woolfrey [17] calculated that during alpha decay in Synroc phases, recoil nuclei and alpha particles cause ~1500 and ~100 displacements respectively, on the basis that the atoms in the displacement cascades behave like primary knock-on atoms produced by external bombardment with fast neutrons and by considering only the first interaction. Van Konynenburg and Guinan [18] calculated that in Synroc phases recoil nuclei and alpha particles cause 980 and 120 displacements, respectively. They assumed that recoils were stopped in monatomic solid made up of the same chemical element as the recoil itself, and used the code written by Guinan in conjunction with the stopping theory of Lindhard et al. [19] and stopping data from Ziegler [20]. Both these approaches have limitations, so we decided to check their calculations using the program Transport of Ions in Materials (TRIM [21]) Version 98.01 in full cascade mode. TRIM uses the binary collision approximation to model the irradiation of target materials with ions. We modelled interactions in target materials perovskite, zirconolite, hollandite and freudenbergite using endmember compositions ($CaTiO_3$, $CaZrTi_2O_7$, $Ba_{1.14}(Al_{2.29}Ti_{5.71})_8O_{16}$ and $Na_2Fe_2Ti_7O_{18}$ respectively) and using Th and He to simulate recoil and alpha particle interactions, respectively. Our results are comparable to those of the previous authors (Table 1).

When simulating alpha recoil damage, TRIM may overestimate D_c (despite the fact that TRIM does not account for recombination events). Results from Cm and Pu-doped zirconolite [22,23] show that D_c (zirconolite) corresponds to ~0.4 dpa whereas TRIM results for natural end-member zirconolite ($CaZrTi_2O_7$) irradiated with 1.5 MeV Kr^+ ions [24] and fabricated end-member zirconolite irradiated with 3 MeV Ar^+ ions [25] suggest that D_c (zirconolite) equals 0.8 [re-calculated by 16] and ~1.5 dpa, respectively.

TRIM modelling of alpha particle irradiation is less easy to assess, but the following data suggest that it is acceptable. Self-irradiated, Pu-doped zircon becomes amorphous at 0.59 dpa whereas natural zircon irradiated with 2 MeV He^+ ions only becomes amorphous at 2.3 dpa [26]. Cm-doped apatite ($Ca_2La_8(SiO_4)_6O_2$) becomes amorphous at 0.4 dpa whereas undoped apatite irradiated with 0.8 MeV Ne^+becomes amorphous 1.39 dpa [27]. These data for zircon and apatite show that amorphisation dose (in dpa) is source dependent and suggest , as one would expect, that many of the vacancies and interstitial displacements caused by alpha particles quickly recombine.

In Section 4.1.3, we use the ratio of the number of displacements caused by recoil nuclei to that caused by α-particles during alpha decay events in Synroc phases, to calculate the total displacement damage in freudenbergite. Given the data discussed in the previous two paragraphs, it is possible that the ratio calculated from our TRIM data (82:18) is skewed and overestimates the amount of damage caused by alpha particles by a factor of approximately two.

4.1.3. Calculations of total alpha decay-induced displacement damage in freudenbergite

Previous authors have shown rare-earth and/or actinide-doped zirconolite [16] and rare-earth doped perovskite [28] become amorphous at doses of $\sim 4 \times 10^{18}$ ions m^{-2}. If one assumes that:

(a) ion irradiation data can be used to predict the behaviour of actinide-bearing phases over long periods of time (see comments in Section 4.3),
(b) perovskite and zirconolite in Synroc-C will each contain approximately half the total actinide inventory,
(c) the actinide content of freudenbergite is negligible (so the displacement damage experienced by freudenbergite due to self-irradiation is negligible),
(d) each freudenbergite grain is surrounded by only perovskite and zirconolite grains (which would expose freudenbergite to the highest possible dose from adjacent grains),
(e) the displacement damage in the periphery of freudenbergite grains due to the incursion of recoil

Table 1
Average number of displacements caused by recoil nuclei and alpha particles in Synroc phases as calculated by TRIM using E_d and E_b values of 15 and 2 eV, respectively

	Perovskite	Zirconolite	Hollandite	Freudenbergite	Average % of total displacements caused by an alpha decay
Calculated density (gm cm^{-3})	4.03	4.44	4.27	4.27	
Average number of displacements caused by recoil nuclei	1774	1856	1784	1882	82.5 ± 2.5
Average number of displacements caused by alpha particles	374	394	358	412	17.5 ± 2.5

nuclei from adjacent actinide-bearing grains is one quarter of that in the adjacent actinide-bearing grains (see Section 4.1.1) and

(f) the alpha particle dose is distributed uniformly over all the phases in Synroc-C (given that the sizes of grains in Synroc-C vary from 0.2 to 1.0 μm and alpha particle travel 10–20 μm),

then at the time zirconolite and perovskite grains become amorphous, the periphery and the centres of freudenbergite grains will have received doses equivalent to $\leqslant 1.5 \times 10^{18}$ ions m^{-2} and $\leqslant 0.72 \times 10^{18}$ ions m^{-2}, respectively (see Table 2). In other words, the calculations in Table 2 suggest that when zirconolite and perovskite become amorphous freudenbergite will still be crystalline. Furthermore, as discussed in Section 4.1.1, the ratio of displacements we calculate from our TRIM data may overestimate the amount of damage caused by alpha particles. Conseqently, the amount of alpha decay damage we calculate at the centre of freudenbergite grains (at the time that zirconolite and perovskite become amorphous) is an upper limit.

The above calculations agree with the X-ray diffraction-based findings of Mitamura and White [29,30], who studied self-irradiation damage of ^{244}Cm-doped Synroc containing Na-rich HLW. In Synroc, which had sustained doses of up to 1.24×10^{18} decay events g^{-1}, Mitamura and White [29,30] found that in (a) damage in all phases increased with dose and (b) the relative damage sustained by the major phases followed the expected distribution of Cm. That is, at any dose, zirconolite and perovskite were less crystalline than hollandite and freudenbergite. It would be informative to do TEM on samples from studies like those of Mitamura and White [29,30] to examine the distribution and level of radiation damage in all the major phases, and in particular in freudenbergite grains, as a function of dose and thermal history.

4.2. D_c values, structural freedom, f, and susceptibility to amorphisation, S

Structural freedom, f, and susceptibility to amorphisation, S, are parameters that have been developed by two groups of authors (Hobbs and coworkers [32–35] and Wang and coworkers [36–41] respectively) to try and predict the relative radiation resistance of different phases. In the following subsections we will define f and S, calculate these parameters for freudenbergite, zirconolite and perovskite and discuss the accuracy of these parameters for predicting the relative radiation resistance of these phases.

4.2.1. Structural freedom

Gupta [31], then Hobbs and coworkers [32–35] suggested that the relative susceptibility to amorphisation of different materials could be predicted from the topology of only their network-forming cations by calculating their structural freedom, f, according to Eq. (7) shown below.

$$f = d - C\{\delta - [\delta(\delta+1)/2V]\} - (d-1)(Y/2) - [(p-1)d - (2p-3)](Z/p), \quad (7)$$

Table 2
Calculations of displacement damage in freudenbergite

Ratio of displacements caused by recoils to that caused by alpha particles in an alpha decay	82:18[a]	89:11[b]	94:6[c]
Dose in periphery of freudenbergite grains due to incursion of recoils from neighbouring grains	$= 82/100 \times 1/4 \times 4 \times 10^{18}$ ions $m^{-2} = 0.82 \times 10^{18}$ ions m^{-2}	$= 89/100 \times \times 4 \times 10^{18}$ ions $m^{-2} = 0.89 \times 10^{18}$ ions m^{-2}	$= 94/100 \times 1/4 \times 4 \times 10^{18}$ ions $m^{-2} = 0.94 \times 10^{18}$ ions m^{-2}
Dose in freudenbergite grains due to transit of alpha particles from neighbouring grains	$= 18/100 \times 4 \times 10^{18}$ ions m^{-2} $= 0.72 \times 10^{18}$ ions m^{-2}	$= 11/100 \times 4 \times 10^{18}$ ions $m^{-2} = 0.44 \times 10^{18}$ ions m^{-2}	$= 6/100 \times 4 \times 10^{18}$ ions m^{-2} $= 0.24 \times 10^{18}$ ions m^{-2}
Total dose in the periphery of freudenbergite grains due to alpha decay events in neighbouring grains	$= 1.5 \times 10^{18}$ ions m^{-2}	$= 1.3 \times 10^{18}$ ions m^{-2}	$= 1.2 \times 4 \times 10^{18}$ ions m^{-2}

[a] This study.
[b] Van Konynenberg and Guinan [18].
[c] Reeve and Woolfrey [17].

where d is the network dimensionality, δ the dimensionality of the structuring polytope (the term polytope generalises the concept of the geometric representation of a coordination unit such as a polygon or a polyhedron to a space of arbitary dimension), C the connectivity (the number of polytopes sharing a vertex), V the number of verticies of the structuring polytope, Y the fraction of edge-sharing verticies, Z the fraction of face-sharing verticies and p is the number of edges of the polytope.

Hobbs et al. [35] compared the measured D_c values (in dpa) and f values (calculated only on the basis of the network-forming cations) of various non-metal phases with the following structure types: AO, AO_2, A_2O_3, ABO_3, ABO_4, $A_2B_2O_7$ and A_2BO_4. They found that f predicted the relative radiation sensitivities of some, but not all phases in their study.

Table 3 compares the D_c, and f values of freudenbergite, zirconolite and perovskite and lists the values of the variables used to calculate the f values. The f values for perovskite and zirconolite (-1 and -0.33, respectively) are taken from Hobbs et al. [35]. The values of the variables Hobbs et al. [35] would have used to calculate these f values are included in Table 3 for completeness. The f value of freudenbergite (-3.16) was calculated on the basis of its (Al,Ti)–O framework using the values listed in Table 3.

f does not correctly predict the relative radiation damage susceptibilities of freudenbergite, zirconolite and perovskite. f predicts that perovskite is more resistant to heavy ion irradiation than zirconolite. While this is true if one compares end member perovskite (containing minor sodium) with end member zirconolite, the D_c of loparite (sodium and rare earth element substituted $CaTiO_3$ perovskite) [28] is less than that of end-member zirconolite ($CaZrTi_2O_7$). f also wrongly suggests that freudenbergite is more resistant to radiation damage than both zirconolite and perovskite, whereas the D_c values of all the zirconolites and perovskites we have measured are greater than D_c (freudenbergite).

4.2.2. Susceptibility to amorphisation, S

Wang and coworkers [36–41] suggested that the susceptibility to amorphisation, S, of a material depends on the topology of its network-forming cations, bond strengths and the upward phase transition temperature. S was originally defined using Eqs. (8)–(11) [28]. In this paper, we calculate S values using both this and a more recent definition, so for clarity we designate values calculated using the original definition as S_o values.

$$S_o = f(T_i)\sum_i \delta_i x_i G_i F_i^c \tag{8}$$

in which

$$G_i = \frac{1}{C_i}\left(\frac{n_{sh}}{n_T}\right)^2, \tag{9}$$

$$F_i = \frac{z_1.z_2}{a_i^2}, \tag{10}$$

$$f(T_i) = \frac{1}{T_s^d}, \tag{11}$$

where δ is the dimensionality of the structuring polytope, x_i the mole fraction of the ith cation (anions are not counted), C_i the connectivity of the ith polytope (the number of polytopes shared at one corner anion and equals the coordination number of the anion), n_{sh} the number of shared polytope corners, n_T the total number of polytope corners for one cation, z_1 and z_2 are the

Table 3
f, the structural connectivity, of freudenbergite, perovskite and zirconolite

Phase polyhedral type	d	δ	V	p	Y	Z	C	f	D_c (10^{18} ions cm^{-2})
Freudenbergite[a] (Ti, Al)–O octahedra	3	3	6	12	0.83′	0	2.66′	−3.16	1.6 ± 0.3
End member zirconolite[b] ($CaZrTi_2O_7$) Ti–O octahedra[c]	3	3	6	12	0	0	1.66′	−0.33	5.5 ± 1.3
Nd−doped zirconolite ($Ca_{0.81}Nd_{0.17}Zr_{1.08}Ti_{1.89}O_7$)[b] Ti–O octahedra[b]	3	3	6	12	0	0	1.66′	−0.33	5.3 ± 0.7
End member perovskite ($CaTiO_3$) Ti–O octahedra	3	3	6	12	0	0	2	−1	
End member perovskite with minor Na (1.2 at.%)[d] Ti–O octahedra	3	3	6	12	0	0	2	−1	9.2 ± 2.4
Loparite[d] (Na & REE substituted $CaTiO_3$) Ti–O octahedra	3	3	6	12	0	0	2	−1	3.9 ± 0.5

[a] From this study.
[b] From Smith et al. [16].
[c] Does not take account of the Ti atoms coordinated to five oxygens.
[d] From Smith et al. [28].

Table 4
D_c and S_o values of freudenbergite, perovskite and zirconolite

Phase description cation	δ	x_i	C_i	n_{sh}	n_T	z_1	z_2	a_i[a]	T_s (K)	S	D_c (10^{18} ions cm^{-2})
Freudenbergite ($NaAl_2Ti_6O_{16}$)[b]										6.85	1.6 ± 0.3
Na	3	0.2	12	8	12	0.083′	0.083′	3.276	1448		
Ti	3	0.8	3	6	6	0.66′	0.66′	1.928	1448		
End member zirconolite ($CaZrTi_2O_7$)[c]										2.42	5.5 ± 1.3
Ca	3	0.25	8	4	8	0.25	0.25	2.452	1798		
Zr	3	0.25	3.5	4	7	0.571	0.571	2.248	1798		
Ti	3	0.50	3	4	6	0.66′	0.66′	1.941	1798		
Zirconolite ($Ca_{0.81}Nd_{0.17}Zr_{1.08}Ti_{1.89}O_7$)[c]										–	5.3 ± 0.7
End member perovskite ($CaTiO_3$)										4.40	
Ca	3	0.5	12	12	12	0.166′	0.166′	2.728	2253		
Ti	3	0.5	3	6	6	0.66′	0.66′	1.956	2253		
End member perovskite with minor (1.2 at.%) Na[d]										–	9.2 ± 2.4
Loparite (Na REE substituted $CaTiO_3$)[d]										–	3.9 ± 0.5

[a] Average bondlength between cation and surrounding anions as determined using CrystalMaker (http://www.crystalmaker.co.uk/index.html).
[b] This study.
[c] Smith et al. [16].
[d] Smith et al. [28].

effective electrostatic charges (equal to the charge of the cation divided by its coordination number, a_i the cation–anion distance T_s is the phase transition temperature (K) and is equivalent to the melting temperature when the phase transition is from solid to liquid as in all ceramics, c and d are constants ($c = 0.3, d = 0.1$). S_o correctly predicted the relative radiation sensitivities of the majority of the phases in the $MgO–Al_2O_3–SiO_2$ system for which D_c had been measured [36].

Recently, Wang et al [40,41] simplified the definition of S, by using the charge neutrality rule and now define S using Eq. (12). However it appears that they have applied the charge neutrality rule to networks of like polyhedra in materials containing more than one cation type, which may or may not be valid. Consequently we have calculated S using both the original and new definitions of susceptibility, S_o and S_n respectively.

$$S_n = 100\frac{1}{2}\frac{1}{T_s^{0.1}}\sum_i\left(x_i\frac{(z_i/N_i)^{1.6}}{a_i^{0.6}}\right), \tag{12}$$

where x_i is the mole fraction of the ith cation, z_i the charge on the ith cation, N_i the coordination number of the ith cation, a_i the cation–anion distance (Å), T_s is the phase transition temperature (K) and is equivalent to the melting temperature when the phase transition is from solid to liquid as in all ceramics. S_n correctly predicts the relative radiation sensitivities of all of the phases in the $MgO–Al_2O_3–SiO_2$ system for which D_c had been measured [41].

Tables 4 and 5 list the S_o and S_n values of freudenbergite, zirconolite and perovskite and the values we substituted into Eqs. (8)–(12) to calculate these values. Only the S_o and S_n values of end-member perovskite ($CaTiO_3$) and zirconolite ($CaZrTi_2O_7$) have been calculated, as the melting points of the non-endmember zirconolite and perovskites are not known.

Tables 4 and 5 compare the D_c, S_o and S_n values of freudenbergite, zirconolite and perovskite. Neither S_o nor S_n correctly predict the relative susceptibilities of all three phases. S_o and S_n values correctly predict that D_c (freudenbergite) is less than D_c (zirconolite) and D_c (perovskite) but incorrectly predict that D_c (zirconolite) is greater than D_c (perovskite).

4.3. Factors affecting D_c: composition and ionic mobility

Various results from the literature suggest that composition and ionic mobility may affect the resistance of phases to ion beam irradiation. Eby et al. [42] found that Na-bearing pyroxene and plagioclase were more susceptible to ion-beam irradiation than non-Na-bearing pyroxene and plagioclase, respectively. Furthermore, it is well known that focussed electron probes in scanning and transmission electron microscopes cause alkali and in particular Na^+ migration in alkali aluminosilicate glasses and minerals, making chemical analyses of these phases difficult (e.g., [43,44]). Such migration is due to long-range electric fields [45]. In thin insulating (or even slightly dielectric) specimens, alkali ions move radially

Table 5
D_c and S_n values of freudenbergite, perovskite and zirconolite

Phase description cation	T_s (K)	x_i	z_i	N_i	a_i[a]	S_n	D_c (10^{18} ions cm^{-2})
Freudenbergite ($NaAl_2Ti_6O_{16}$) [b]						6.85	1.6 ± 0.3
Na	1448	0.2	0.083′	12	3.276		
Al, Ti	1448	0.8	0.66′	6	1.928		
End member zirconolite ($CaZrTi_2O_7$) [c]						3.15	5.5 ± 1.3
Ca	1798	0.25	0.25	8	2.452		
Zr	1798	0.25	0.571	7	2.248		
Ti	1798	0.50	0.66′	4	1.941		
Zirconolite ($Ca_{0.81}Nd_{0.17}Zr_{1.08}Ti_{1.89}O_7$)						–	5.3 ± 0.7
End member perovskite ($CaTiO_3$)						6.61	
Ca	2253	0.5	0.166′	12	2.728		
Ti	2253	0.5	0.66′	6	1.956		
End member perovskite with minor (1.2 at.%) Na [d]						–	9.2 ± 2.4
Loparite (Na & REE substituted $CaTiO_3$)[d]						–	3.9 ± 0.5

[a] Average bondlength between cation and surrounding anions as determined using CrystalMaker (http://www.crystalmaker.co.uk/index.html).
[b] This study.
[c] Smith et al. [16].
[d] Smith et al. [28].

outward from the area of contact of the electron beam because of the excess production of secondary electrons at the surface. The alkali ions are then redistributed within the sample according to their respective mobilities. Na^+, in particular, is highly mobile. Irradiation of TEM specimens by Kr^+ ions will also cause production of secondary electrons which could result in local short lived charge imbalance, in turn causing ionic mobility. Consequently, the low value of D_c (freudenbergite) measured in this study may be due, in part, to the high mobility of Na^+ ions in Kr^+ ion-induced electric fields in the freudenbergite TEM specimens.

The possibility that local short lived charge imbalance exists in TEM specimens during heavy ion irradiation suggests that caution should be exercised when using heavy ion irradiation as a simulant of alpha decay damage. Particularly if heavy ion irradiation is being used to assess the relative radiation resistance of: (i) different phases and (ii) samples with the same structure but different compositions, especially if the samples contain differing amounts of alkali elements.

In TRIM calculations of dpa, most authors, including ourselves use one E_d value for all the elements in a phase. Few E_d values have been directly measured. If heavy ion irradiation causes electric fields in TEM specimens, separate E_d values for each element may need to be used in TRIM calculations and measurements of E_d may need to be made in conditions which mimic the field(s) generated by heavy ion irradiation.

The possibility that heavy ion irradiation causes electric fields in TEM specimens also has consequences for the current amorphisation susceptibility indicators. Neither f nor S directly take account of composition or ionic mobility. f depends solely on topology while S depends on the topology, bond strengths and melting temperature of a phase. The formulae for f and S may need to be modified to include ionic mobility.

5. Conclusions

In this study, D_c (freudenbergite) was found to be $1.6 \pm 0.3 \times 10^{18}$ ions m^{-2}. This is lower than D_c (zirconolite) and D_c (perovskite) (3.5–5.5 and 3.9–9.2 $\times 10^{18}$ ions m^{-2} respectively) [16,28].

In agreement with the experimental findings of previous authors [29,30], calculations show that in Synroc-C, freudenbergite will remain crystalline after zirconolite and perovskite have become amorphous.

Neither of the two current models for estimating the relative radiation resistance of different phases is capable of predicting the relative radiation resistance of freudenbergite, zirconolite and perovskite. Freudenbergites low D_c value may be due to electric field-induced movement of Na^+ ions.

Acknowledgements

The authors thank the HVEM-Tandem Facility staff at Argonne National Laboratory for assistance during ion irradiations, particularly Charlie Allen, Ed Ryan, Stan Ockers, Tony McCormick, Pete Baldo and Lauren Funk. The Facility is supported as a User Facility by the US DOE, Basic Energy Sciences, under contract W-31-109-ENG-38. The authors also thank Lou (E.R.)Vance for providing the freudenbergite sample, Bill (W.K.) Bertram for assistance with mathematical modelling. Mike Colella for desktop publishing assistance and Sammy Leung for assistance with SEM/EDS data acquisition. The structures of freudenbergite, perovskite and zirconolite were analysed using CrystallMaker 2.0: A crystal structures program for MacOS Computers (http://www.crystalmaker.co.uk).

References

[1] R.C. Ewing, W.J. Weber, F.W. Clinard Jr., Progr. Nucl. Energy 29 (1995) 63.
[2] B.M. Gatehouse, I.E. Grey, R.J. Hill, H.J. Rossell, Acta Crystallogr. B 37 (1981) 306.
[3] H.J.A. Koopmans, G.M.H. Van de Velde, P.J. Gellings, Acta Crystallogr. C39 (1983) 1323.
[4] J.A. Cooper, D.R. Cousens, J.A. Hanna, R.A. Lewis, S. Myhra, R.L. Segall, R.St.C. Smart, T.J. White, J. Am. Ceram. Soc. 69 (1986) 347.
[5] W.J. Buykx, K. Hawkins, D.M. Levins, H. Mitamura, R.St.C. Smart, G.T. Stevens, K.G. Watson, D. Weedon, T.J. White, J. Am. Ceram. Soc. 71 (1988) 678.
[6] W.J. Buykx, D.M. Levins, R.St.C. Smart, K.L. Smith, G.T. Stevens, K.G. Watson, T.J. White, J. Am. Ceram. Soc. 73 (1990) 217.
[7] E.R. Vance, M.W.A. Stewart, G.R. Lumpkin, J. Mater. Sci. 26 (1991) 2694.
[8] G.R. Lumpkin, K.L. Smith, M.G. Blackford, J. Nucl. Mater. 224 (1995) 31.
[9] G. Frenzel, Ein neues Mineral: Freudenbergit (Na2Fe2-Ti7O18), Neues Jarb. Mineral., Monatsh. 1 (1961) 12.
[10] S. Andersson, A.D. Wadsley, Acta Crystallogr. 15 (1062) 201.
[11] E.R. Vance, P.J. Angel, D.J. Cassidy, M.W.A. Stewart, M.G. Blackford, P.A. McGlinn, J. Am. Ceram. Soc. 77 (1994) 1576.
[12] G.T. Thorogood, E.R. Vance, J. Am. Ceram. Soc. 74 (1991) 854.
[13] Irradiation Effects in Nuclear Waste Forms, Summary Report PNL-3588. Pacific Northwest Laboratories, Richland Wa (1981).
[14] M.R. Pascucci, J.L. Hutchison, L.W. Hobbs, Radiat. Eff. 74 (1983) 219.
[15] M.G. Blackford, Comparison of EDS performance before and after replacement of a Tracor Northern Microanalyser with a Link ISIS, Proceedings of Third Biennial Symp. on SEM Imaging and Analysis: Applications and Techniques,

15–17 February 1995, University of Melbourne, 1997, p. 98.
[16] K.L. Smith, G.R. Lumpkin, N.J. Zaluzec, J. Nucl. Mater. 250 (1997) 36.
[17] K.D. Reeve, J.L. Woolfrey, J. Austral. Ceram. Soc. 16 (1980) 10.
[18] R.A. Van Konynenburg, M.W. Guinan, Nucl. Tech. 60 (1983) 206.
[19] J. Lindhard, V. Nielsen, M. Scharff, P.V. Thomsen, Mater. Fys. Medd. Dan. Vid. Selsk. 33 (1963) 1.
[20] J.F. Ziegler, Helium: Stopping Powers and Ranges in all Elemental Matter, Pergamon, New York, 1977, p. 66.
[21] J. Ziegler, J.P. Biersack, U. Littmark, The Stopping Range of Ions in Solids, Pergammon, New York, 1985.
[22] Weber, J.W. Wald, Hj. Matzke, J. Nuc. Mater. 138 (1986) 196.
[23] F.W. Clinard Jr., D.L. Rohr, R.B. Roof, Nuc. Instrum. and Meth. B 1 (1984) 581.
[24] R.C. Ewing, L.-M. Wang, Nucl. Instrum. and Meth. B 65 (1992) 319.
[25] W.J. Weber, N.J. Hess, G.D. Maupin, Nucl. Instrum. and Meth. B 65 (1992) 102.
[26] W.J. Weber, R.C. Ewing, L.-M. Wang, J. Mater. Res. 9 (1994) 688.
[27] W.J. Weber, R.C. Ewing, L.-M. Wang, Nucl. Instrum. and Meth. B 91 (1994) 63.
[28] K.L. Smith, G.R. Lumpkin, M.G. Blackford, N.J. Zaluzec, Mater. Res. Soc. Symp. Proc. 540 (1999) 323.
[29] H. Mitamura, S. Matsumoto, T. Miyazaki, T.J. White, K. Nukaga, Y. Togashi, T. Sagawa, S. Tashiro, D.M. Levins, A. Kikuchi, J. Am. Ceram. Soc. 73 (1990) 3433.
[30] T.J. White, H. Mitamura, K. Hojou, S. Furuno, Mater. Res. Soc. Symp. Proc. 333 (1994) 227.
[31] P.K. Gupta, J. Am. Ceram. Soc. 76950 (1993) 1088.
[32] L.W. Hobbs, Nucl. Instrum. and Meth. B 91 (1994) 30.
[33] L.W. Hobbs, J. Non-Cryst. Solids 182 (1995) 27.
[34] L.W. Hobbs, J. Non-Cryst. Solids 193 (1995) 79.
[35] L.W. Hobbs, A.N. Seeram, C.E. Jesurum, B.A. Berger, Nuc. Instrum. and Meth. B 116 (1996) 18.
[36] S.X. Wang, L.M. Wang, R.C. Ewing, Mater. Res. Soc. Symp. Proc. 439 (1997) 619.
[37] S.X. Wang, L.M. Wang, R.C. Ewing, Nucl. Instrum. and Meth. B 127/128 (1997) 186.
[38] L.M. Wang, S.X. Wang, W.L. Gong, Mater. Res. Soc. Symp. Proc. 439 (1997) 583.
[39] S.X.Wang, Pers. Comm. (1997).
[40] S.X. Wang, L.M. Wang, R.C. Ewing, R.H. Doremus, J. Non-Cryst. Solids 238 (1998) 195.
[41] S.X. Wang, L.M. Wang, R.C. Ewing, R.H. Doremus, J. Non-Cryst. Solids 238 (1998) 214.
[42] R. Eby, R.C. Ewing, R.C. Birtcher, J. Mater. Res. 7 (1992) 3080.
[43] G.B. Morgan VI, D. London, Am. Mineral 81 (1996) 1176.
[44] D.G. Howitt, D.L. Medlin, Proceedings of the Microscopy Society of America Annual Meeting, 1998.
[45] T.M. Walker, D.G. Howitt, Scanning 11 (1998) 5.